Insights into Brain Glycogen Metabolism

Cécile Mathieu, Ines Li de La Sierra-Gallay, Romain Duval, Ximing Xu, Angélique Cocaign, Thibaut Léger, Gary Woffendin, Jean-Michel Camadro, Catherine Etchebest, Ahmed Haouz, et al.

THE JOURNAL OF BIOLOGICAL CHEMISTRY VOL. 291, NO. 35, pp. 18072–18083, August 26, 2016

Insights into Brain Glycogen Metabolism

THE STRUCTURE OF HUMAN BRAIN GLYCOGEN PHOSPHORYLASE[*S]

Received for publication, May 18, 2016, and in revised form, July 7, 2016 Published, JBC Papers in Press, July 8, 2016, DOI 10.1074/jbc.M116.738898

Cécile Mathieu[a1], Ines Li de la Sierra-Gallay[b], Romain Duval[a2], Ximing Xu[a3], Angélique Cocaign[a1], Thibaut Léger[c], Gary Woffendin[d], Jean-Michel Camadro[c], Catherine Etchebest[e,f,g,h,i], Ahmed Haouz[j], Jean-Marie Dupret[a,i], and Fernando Rodrigues-Lima[a,i4]

From the [a]Université Paris Diderot, Sorbonne Paris Cité, Unité BFA, CNRS UMR 8251, 75013 Paris, France, the [b]Fonction et Architecture des Assemblages Macromoléculaires, Institut de Biologie Intégrative de la Cellule, Université Paris Sud, UMR 9198 Orsay, 91405 France, the [c]Université Paris Diderot, Sorbonne Paris Cité, Institut Jacques Monod, CNRS UMR 7592, 75013 Paris, France, [d]Thermo Fisher Scientific, Hemel Hempstead HP2 7GE, United Kingdom, [e]INSERM, UMR S1134, Université Paris Diderot, 75015 Paris, France, [f]Université Paris Diderot, Sorbonne Paris Cité, 75004 Paris, France, [g]Institut National de la Transfusion Sanguine, 75015 Paris, France, [h]Laboratoire d'Excellence GR-Ex, 75015 Paris, France, [i]UFR Sciences du Vivant, Université Paris Diderot, 75013 Paris, France, and the [j]Institut Pasteur, Plateforme de Cristallographie, CNRS UMR 3528, 75015 Paris, France

Brain glycogen metabolism plays a critical role in major brain functions such as learning or memory consolidation. However, alteration of glycogen metabolism and glycogen accumulation in the brain contributes to neurodegeneration as observed in Lafora disease. Glycogen phosphorylase (GP), a key enzyme in glycogen metabolism, catalyzes the rate-limiting step of glycogen mobilization. Moreover, the allosteric regulation of the three GP isozymes (muscle, liver, and brain) by metabolites and phosphorylation, in response to hormonal signaling, fine-tunes glycogenolysis to fulfill energetic and metabolic requirements. Whereas the structures of muscle and liver GPs have been known for decades, the structure of brain GP (bGP) has remained elusive despite its critical role in brain glycogen metabolism. Here, we report the crystal structure of human bGP in complex with PEG 400 (2.5 Å) and in complex with its allosteric activator AMP (3.4 Å). These structures demonstrate that bGP has a closer structural relationship with muscle GP, which is also activated by AMP, contrary to liver GP, which is not. Importantly, despite the structural similarities between human bGP and the two other mammalian isozymes, the bGP structures reveal molecular features unique to the brain isozyme that provide a deeper understanding of the differences in the activation properties of these allosteric enzymes by the allosteric effector AMP. Overall, our study further supports that the distinct structural and regulatory properties of GP isozymes contribute to the different functions of muscle, liver, and brain glycogen.

Glycogen performs various functions depending on its location in the body. In muscle, glycogen provides energy via the glycolysis pathway for skeletal muscle contraction (1, 2). Liver glycogen is metabolized and subsequently released as glucose into systemic circulation during fasting periods (1, 2). Brain glycogen has long been considered to be an emergency glucose store (1, 2). The key roles that brain glycogen and its metabolism play in the mammalian nervous system have only emerged over the last 20 years (3–5). For instance, astrocyte function and neuronal activity are critically dependent on glycogen stores and glycogenolysis, especially during episodes of stress including hypoglycemia and ischemia (6–9). Astrocytic glycogen breakdown and subsequent astrocyte-neuron lactate transport have also been proposed to support high cognitive processes such as learning and memory consolidation (10–16). In addition, glycogen metabolism in neurons participates in neuronal tolerance to hypoxic stress (17). Glycogen itself is also important for brain function. However, alteration of its metabolism and overaccumulation in the brain, such as in Lafora disease, contributes to neurodegeneration (16, 18, 19).

Glycogen phosphorylase (EC 2.4.1.1; GP)[5] is the key enzyme that regulates glycogen mobilization. This complex allosteric enzyme catalyzes the rate-limiting step of glycogenolysis by releasing glucose-1-phosphate (1). In mammals, GP comprises a family of three isozymes named according to the tissue of their highest abundance: muscle isozyme (mGP), liver isozyme (lGP), and brain isozyme (bGP). The three isozymes form homodimers comprised of identical subunits that are encoded by distinct but structurally related genes (20–22). GPs are allosteric enzymes that are regulated by both phosphorylation of Ser^{14} and binding of allosteric effectors (such as AMP) that control their transition between inactive and active conformations (1). Although GPs display high similarity and catalyze the same reaction, these three isozymes differ in their sensitivity to allosteric activation and phosphorylation (1, 23, 24): lGP is essentially regulated by phosphorylation, mGP responds cooperatively to activation by AMP and to phosphorylation, and

* This work was supported by running grants from University Paris Diderot, CNRS, and Institut Pasteur. The authors declare that they have no conflicts of interest with the contents of this article.
[S] This article contains supplemental Tables S1 and Figures S1 and S2.
The atomic coordinates and structure factors (codes 5IKP and 5IKO) have been deposited in the Protein Data Bank (http://wwpdb.org/).
[1] Supported by Ph.D. fellowships from the French Ministry of Research (Ecole Doctorale BioSPC).
[2] Supported by a Ph.D. fellowship from Région Ile de France (appel hors DIM 2013).
[3] Supported by a fellowship from the China Scholarship Council. Present address: Institut Pasteur, Unité de Pathogénèse des Infections Vasculaires, 75015 Paris, France.
[4] To whom correspondence should be addressed. E-mail: fernando.rodrigues-lima@univ-paris-diderot.fr.

[5] The abbreviations used are: GP, glycogen phosphorylase; mGP, muscle GP; lGP, liver GP; bGP, brain GP; PDB, Protein Data Bank.

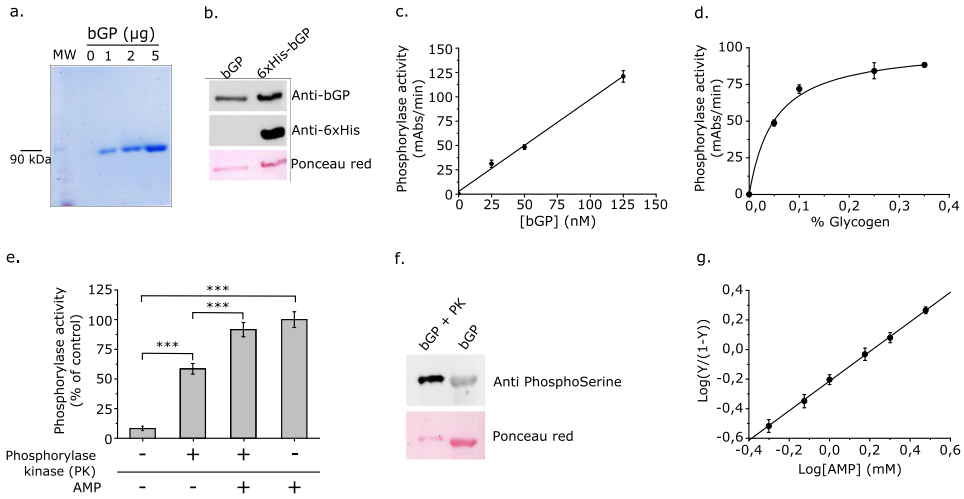

FIGURE 1. **Biochemical characterization of recombinant human bGP.** *a*, SDS-PAGE analysis of purified bGP. 1, 2, and 5 μg of purified bGP were subjected to SDS-PAGE under reducing conditions and stained with Coomassie Blue. *b*, Western blotting analysis of untagged and His_6-tagged bGP. Western blotting analysis was first conducted using a polyclonal antibody against the six-histidine tag and then reprobed using a monoclonal antibody against bGP. *c*, plot of the activity of glycogenolysis as a function of the purified bGP concentration. Various concentrations of purified protein were assayed for enzymatic activity in the direction of glycogen breakdown in the presence of 1 mM AMP and 0.25% glycogen. The data represent the averages of initial velocities (expressed as mAbs/min) of three experiments ± S.D. The curve was fitted to the data using linear regression. *d*, glycogen saturation curve of purified bGP. Purified recombinant bGP (100 nM) activity was measured in the direction of glycogen breakdown in the presence of a saturating concentration of AMP (1 mM) and various concentrations of glycogen (0–0.35%). The data shown represent the means of initial velocities of three different experiments (expressed as mean Abs/min ± S.D.). *e*, activation of bGP by phosphorylation and AMP. Specific phosphorylation of bGP Ser^{14} was performed prior to the assay by incubating the recombinant enzyme with phosphorylase kinase in the presence of ATP for 2 h at room temperature. bGP and phosphorylated bGP was then assayed for activity with or without 1 mM AMP. Activity was expressed as the percentage of the control (bGP activity in the presence of AMP alone). The data shown represent the means of initial velocities of three different experiments ± S.D. ***, $p < 0.001$. *f*, Western blotting of phosphorylated and non-phosphorylated bGP. Recombinant bGP was incubated with (*lane 1*) or without (*lane 2*) phosphorylase kinase and subjected to Western blotting analysis using an anti-phosphoserine antibody. The presence of purified protein was assessed by Ponceau red staining. *g*, non-cooperative binding of AMP. bGP activity was measured in the presence of various concentrations (0–3 mM) of AMP and a saturating concentration of glycogen (0.25%). Initial velocities were determined and fitted to the Hill equation. The resulting n_{Hill} was equal to 0.994, indicating non-cooperative binding of AMP to bGP as previously reported (23). *MW*, molecular weight.

bGP responds strongly and non-cooperatively to activation by AMP (23, 24). These regulatory differences likely represent distinct functions of glycogen metabolism. Activation by AMP provides a response to intracellular energy demand, whereas the enzymatic cascade leading to phosphorylation of GP is the result of extracellular signals (1). Crystallographic determination of the structures of mGP in 1976 and 1992 and lGP in 2000 led to a better understanding of the structural bases for the regulation of these isoenzymes and the development of drugs (25–32). The structure of a mammalian bGP has not been yet determined even though glycogen and bGP are increasingly recognized to play key roles in brain function. Knowledge of the structure of bGP would allow a better understanding of the molecular basis of brain glycogen metabolism, its regulation, and its role in physiological and pathological brain processes. In addition, the structure of bGP could be helpful to design isozyme-specific drugs.

Here, we report the first structures of human bGP in complex with PEG 400 and in complex with AMP, its allosteric activator. These structures demonstrate that bGP has a closer structural relationship with mGP, which is also activated by AMP, contrary to liver GP, which is not. More importantly, the bGP structures suggest the molecular bases responsible for the distinct responses of mGP and bGP to allosteric activation by AMP. More broadly, our study further supports that the distinct structural and regulatory properties of GP isozymes contribute to the different functions of muscle, liver, and brain glycogen.

Results

Biochemical Characterization of bGP—Human bGP was overexpressed in *Escherichia coli* expressing the chaperonin complex GroEL-GroES. The co-expression of the GroEL-GroES complex and human bGP substantially increased the production and purification yield of the functional recombinant enzyme by improving the correct folding of human bGP. The enzyme was expressed as an N-terminal polyhistidine-tagged fusion protein and purified using Ni^{2+} affinity chromatography. The polyhistidine tag was removed by thrombin digestion to ensure structural integrity and full biological activity of the protein. We assessed the protein for purity, enzymatic activity, and full-length sequence (Fig. 1, *a–c*, and supplemental Fig. S1).

GPs are allosteric enzymes activated by both phosphorylation of Ser^{14} by phosphorylase kinase and binding of allosteric effectors, such as AMP. We carried out biochemical and enzymatic characterization of the recombinant bGP to ensure that the purified enzyme was functional. The glycogen saturation curve (Fig. 1*d*) and the activation of the enzyme by AMP, as well as following phosphorylation by phosphorylase kinase (Fig. 1*e*), confirmed the functionality of the protein. We assessed the phosphorylation state of the enzyme by Western blotting, using an antibody raised against phosphorylated serine (Fig. 1*f*) and native mass spectrometry analysis and confirmed the presence of two phosphate groups per dimer (supplemental Fig. S1). Phosphorylation of bGP promoted the activation of the enzyme

TABLE 1
Data collection and refinement statistics

	PEG-bound bGP	AMP-bound bGP
PDB code	5IKO	5IKP
Data collection	3/12/2015	5/16/2015
Beamline	Proxima1	ID23-2
Wavelength (Å)	0.98011	0.8729
Space group	P622	P622
Unit cell dimensions		
a, *b*, *c* (Å)	171.66, 171.66, 122.82	172.0, 172.0, 123.6
α, β, γ (°)	90.0, 90.0, 120.00	90.0, 90.0, 90.00
Resolution (Å)[a]	47.37–2.5 (2.6–2.5)	47.56–3.4 (3.6–3.4)
Completeness (%)	99.2 (98.2)	99.7 (98.8)
Multiplicity	26.4 (26.2)	19.4 (20.3)
$<I/\sigma(I)>$	20.3 (1.14)	27.6 (3.17)
$CC^{1/2}$	99.9 (86.4)	100 (89.2)
R_{merge}[b]	0.12 (1.25)	0.11 (0.93)
Number of reflections	984,486 (152,687)	297,688 (48,355)
Number of unique reflections	37,317 (5835)	15,352 (2385)
Wilson B factor (Å^2)	64.2	112.6
Refinement		
Resolution (Å)[b]	47.37–2.5 (2.6–2.5)	47.56–3.4 (3.5–3.4)
R_{work}	0.187 (0.307)	0.202 (0.291)
R_{free}	0.239 (0.415)	0.295 (0.378)
Number of non-hydrogen atoms	6679	6556
Protein	6547	6535
Others	41	23
Water	84	
ESU (Å)[c]	0.26	0.69
RMSD bonds (Å)	0.013	0.015
RMSD angles (°)	1.6	1.6
Ramachandran favored (%)	96.2	92.5
Ramachandran allowed (%)	3.0	6.3
Ramachandran outliers (%)	0.8	1.2
Average B-factor (Å^2)	69	121.5
Protein (Å^2)	66.8	121.5
Others (Å^2)	86.0	134.8
Water (Å^2)	57.3	

[a] Statistics for highest resolution shell are shown in parentheses.
[b] $R_{merge} = \Sigma_h\Sigma_i|I_{hi} - <I_h>|/\Sigma_h\Sigma_i I_{hi}$, where I_{hi} is the *i*th observation of the reflection *h*, whereas $<I_h>$ is the mean intensity of reflection *h*.
[c] Estimated overall coordinate error based on R_{free} value.

TABLE 2
RMS deviation of GP dimers and monomers in complex with AMP (values in Å)

GP in complex with AMP	mGP (1PYG)	lGP (1FA9)	bGP (5IKP)
GP dimers			
mGP (PDB code 1PYG)		0.71	0.71
lGP (PDB code 1FA9)			0.7
bGP (PDB code 5IKP)			
GP monomers			
mGP (PDB code 1PYG)		0.63	0.69
lGP (PDB code 1FA9)			0.7
bGP (PDB code 5IKP)			

to 60% of that of the control with AMP. The addition of AMP to phosphorylated bGP resulted in a similar level of enzyme activation as that by AMP alone (Fig. 1*e*). We incubated the recombinant enzyme with increasing concentrations of AMP and fitted the initial velocities to the Hill equation to determine whether the binding of AMP to bGP is cooperative. The resulting n_{Hill} coefficient of 0.994 indicated that AMP binding to bGP was not cooperative (Fig. 1*g*). All these characteristics are in accordance with previously published data (23, 24). We thus used this functional enzyme for further crystallographic studies.

The Overall Structure of bGP—We performed several trials to obtain the human bGP structure in its active and inactive conformations. We first attempted to crystallize the enzyme alone and complexed with allosteric effectors such as AMP, ATP, caffeine, glucose, or ammonium sulfate. We obtained bGP crystals in 0.2 M calcium chloride dihydrate, 0.1 M NaHepes, pH 7.5, using 28% (v/v) PEG 400 as precipitant. We did not obtain bGP co-crystals with ligands, despite the high number of crystallization conditions tested. We thus performed soaking experiments of the bGP crystals with several allosteric effectors. Finally, we collected diffraction data sets from bGP crystals, at 2.5 Å resolution and from bGP in complex with AMP at 3.4 Å resolution. The three-dimensional structures were determined by molecular replacement, using a homology model based on human muscle glycogen phosphorylase (PDB code 1Z8D) as a search model (Table 1). bGP shares a high percentage of amino acid sequence identity with the muscle (83%) and liver (80%) isozymes. Accordingly, bGP displays a global structure similar to the other isoforms with monomer and dimer RMSD in alpha carbon positions of <1 Å (Table 2). In both crystals, we have one molecule by asymmetric unit, but a bGP tetramer is formed by crystallographic symmetry (Figs. 2*a* and 3*a*). The tetrameric arrangement of GPs has only been observed for the activated (or R state) of mGP (in the presence of AMP and/or when phosphorylated). In the absence of AMP or phosphorylation, mGP crystallizes as a dimer in the asymmetric unit (PDB code 2GPB). It was thus surprising to observe that in absence of AMP, bGP also formed a tetramer. We attribute this quaternary arrangement to the presence of a PEG 400 molecule, used as precipitant, in the AMP binding site (supplemental Fig. S2) (see "Results" and "Discussion"). Each tetramer is composed by the association of two functional dimers that interact through the catalytic face located at the tetramer interface (29). The regulatory face on the other side is exposed to the solvent (Fig. 2, *b* and *c*). The monomer is composed of two domains: the N-terminal domain from residues 22 to 484 and the C-terminal domain from residues 485 to 822 (Fig. 2, *b* and *c*). The catalytic site, found at the interface between the two domains, is marked by the presence of the electron density of the co-factor pyridoxal phosphate attached to the protein through a Schiff base linkage to Lys^{680}, as observed in the mGP and lGP structures (27–29). Several loops are unstructured in the two bGP structures, including the N-terminal extremity (residues 1–21), the gate loop (residues 285 and 286), and the adenine loop (residues 319–324).

A comparison of the AMP-bound and PEG-bound bGP crystal structures reveals that the two structures are globally similar, with an RMSD of 0.5 Å (Fig. 3*b*). Surprisingly, both the AMP-bound and PEG-bound bGP structures display classical features attributed to the active state of GPs including the open gate loop, the tetrameric association mentioned above, the overall relationship between the dimers, and the conformation of the tower helices (27, 28). These are distinguishing features for the active form of mGP and are consistent with bGP regulation being similar to that of mGP. A PEG 400 molecule is found in the AMP-binding site of PEG-bound bGP structure (Fig. 4*a* and Fig. 3) and interacts with residues involved in the binding of AMP (Fig. 4*b*). The PEG 400 molecule may mimic the binding of AMP and stabilizes the protein in active-like structural conformation. However, we found PEG 400 to be a very poor activator of bGP (data not shown).

The structure of the bGP complexed with AMP was obtained by long time soaking of protein crystals with AMP (supplemental Fig. S2). We suppose that the protein conformation

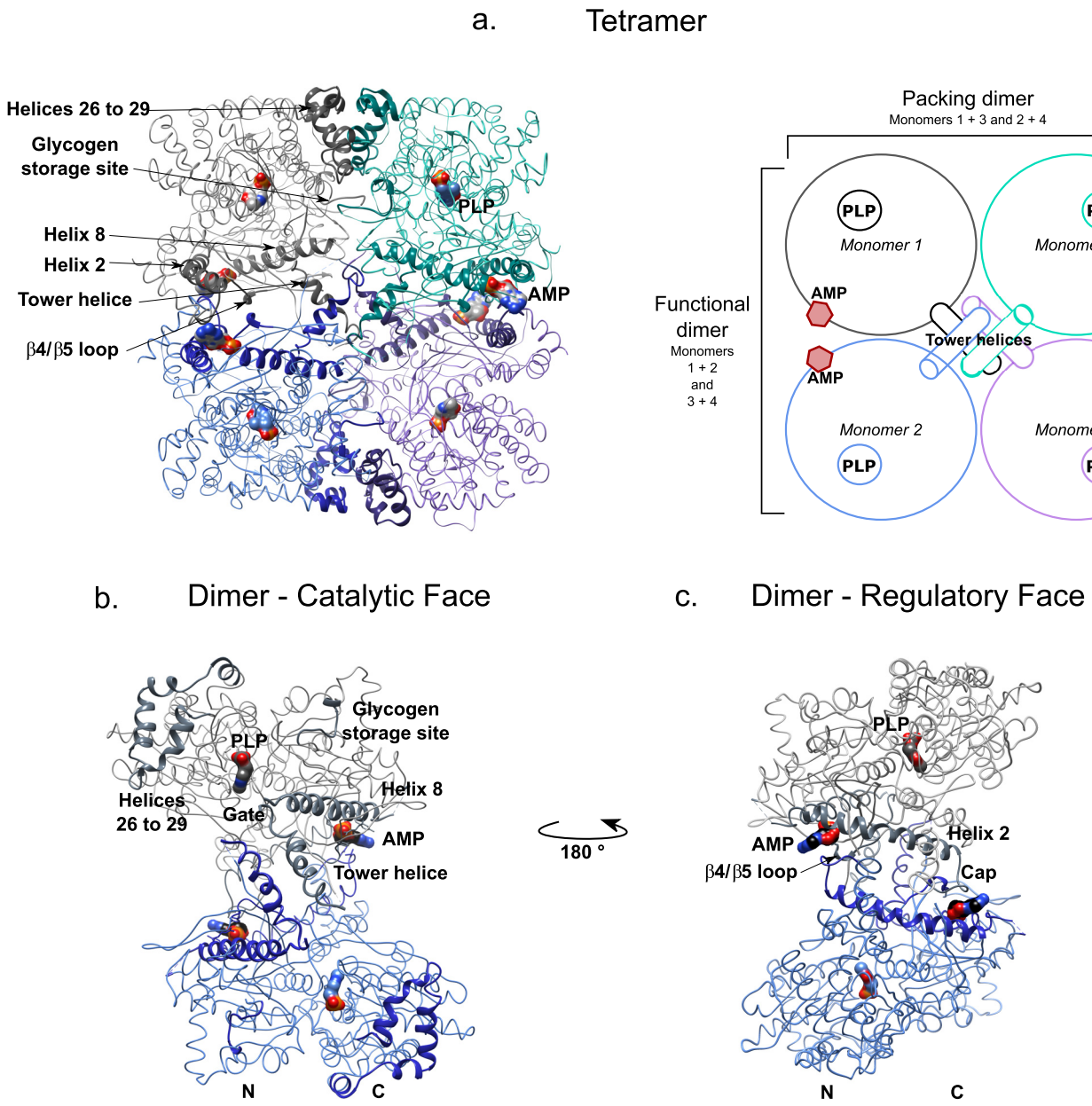

FIGURE 2. **Overview of the structure of AMP-bound brain glycogen phosphorylase.** Shown are schematic and ribbon representations of the C_α trace of the tetramer and functional dimer of bGP. Key secondary structures described in this study are indicated. The catalytic site and the AMP-binding site are marked by the co-factor pyridoxal phosphate and allosteric effector AMP (surface representation), respectively. *a*, the tetrameric organization of bGP. Two bGP monomers associate by the *horizontal axis* to form the functional dimer (monomers 1 and 2). The tetramer is composed of two functional dimers that interact through their catalytic faces, by the *vertical axis*. The association of two monomers through the catalytic site forms the packing dimer (monomers 1 and 3). A schematic representation of the tetramer is shown (*right panel*). The functional dimer corresponds to the association of monomers 1 and 2 (*gray* and *blue*) and monomers 3 and 4 (*turquoise* and *purple*). The packing dimer corresponds to the association of monomers 1 and 3 (*gray* and *turquoise*) and monomers 2 and 4 (*blue* and *purple*). *b*, the catalytic face of bGP. The residues implied in the activation of GP and the subunit interfaces are indicated. The gate loop (residues 279–289) is not stabilized allowing the glycogen to access the catalytic site. The tower helix interacts with its counterparts from the other subunits. The crossover angle of the tower helices in the functional dimer avoids the stabilization of the gate, promoting the opening of the catalytic site. *c*, the regulatory face of bGP contains key regions involved in the control of allosteric transition of the enzyme and is exposed to solvent in both the tetramer and the dimer. *PLP*, pyridoxal phosphate.

observed in PEG-bound bGP crystals is sufficiently close to the active state to allow all the structural changes induced by the addition of AMP without altering the crystal integrity. Indeed, soaking experiments with allosteric inhibitors, such as ATP or caffeine, altered the crystal integrity within seconds (visible cracks and poor diffraction). By contrast, several diffraction data sets were collected from crystals of AMP-complexed bGP obtained by soaking, and the solved structures were similar (monomer RMSD of 0.34 Å and dimer RMSD of 0.35 Å). Changes induced by the addition of AMP were conserved in all the AMP-bound bGP structures. Additionally, the correct and reproducible coordination of AMP in the AMP-binding site and the slight structural changes accompanying PEG 400 replacement by AMP (Fig. 4*c*) suggest that the AMP-bound bGP structure corresponds to the active conformation of the enzyme.

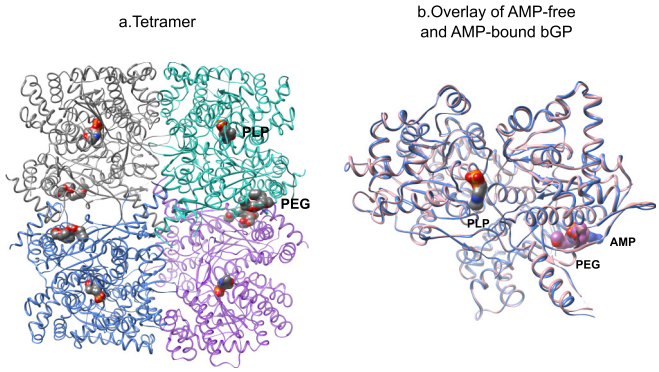

FIGURE 3. **The overall structure of AMP-free bGP.** *a*, AMP-free bGP forms a tetramer, obeying a 222 symmetry, similarly to AMP-bound bGP. PEG400, used as precipitant for crystallization, is found in the AMP binding site. *b*, structural alignment of AMP bound and AMP free monomers. View of the catalytic face of both structures. The catalytic site is marked by the pyridoxal phosphate (*PLP*; surface representation). AMP (*blue*) or PEG 400 (*purple*) is found in the AMP binding site and shown by surface representation.

The Subunit Interfaces—GPs are generally found in two major oligomeric states: dimer and tetramer. In the absence of AMP or phosphorylation, the dimer remains in an inactive conformation. The subunit interfaces of the dimer are remodeled upon activation, allowing the transition from the inactive (T state) to the active (R state) conformations. The remodeling of the mGP interfaces allows this isozyme to form tetramers in which the catalytic sites are occluded (27, 33). The active form of lGP remains as a dimer because of its more rigid structure (29). To confirm the oligomeric state of inactive and active bGP in solution, we performed DLS experiments. We observed that bGP is found as an equilibrium between a monomeric and dimeric form, which is shift toward the dimeric state upon activation (supplemental Table S1). In crystals, bGP forms a tetramer displaying three distinct interfaces, similar to the muscle isoform. Each monomer displays a series of contacts allowing it to interact with the three other monomers of the tetramer. We designate the three interfaces as: 1) the functional dimer, which corresponds to the active dimer (horizontal axis composed of monomers 1 and 2, as well as monomers 3 and 4); 2) the packing dimer, located at the interface between two dimers from the tetramer (vertical axis, composed of monomers 1 and 3, as well as monomers 2 and 4); and 3) the core of the tower helices (Fig. 2*a*).

The Functional Dimer Interface of bGP—We found that the association of two GP monomers into the functional dimer involves helix 2 (residues 49–77), the β4/β5 loop (residues 180–198), the cap′ loop (residues 41–48), and the tower helices (residues 259–278), as observed for mGP and lGP (Fig. 5, *a* and *b*). The helix 2-β4/β5 loop-cap′ loop interface includes the AMP-binding site (Fig. 5*a*). As stated previously, the AMP-binding site in the PEG-bound bGP structure is occupied by a PEG 400 molecule (supplemental Fig. S2 and Fig. 4). The PEG 400 molecule was found to interact with several amino acids involved in the binding of AMP (see below). PEG 400 also interacted with amino acids involved in the functional dimer interface (Fig. 4*a*). The presence of AMP in the AMP-bound bGP structure promoted the formation of specific contacts by concerted movements of amino acid side chains and slight packing of the AMP-binding site around AMP relative to PEG-bound bGP (Fig. 4, *b* and *c*). These movements facilitate interactions between the two subunits by bringing the cap′ loop closer to helix 2 and the β4/β5 loop and stabilize the enzyme in the active conformation (Fig. 5*a*).

The tower helices consist of the anti-parallel association of helix 7 with its symmetric equivalent. The helices are connected to the gate loop (residues 279–289). The gate loop adopts either an open or a closed configuration depending the activation state of the enzyme (27–29) (active or inactive). We found that the helices present a crossover angle of 85° in both the free and AMP-complexed forms (Fig. 5*b*), promoting the open conformation of the gate loop in a manner similar to that previously observed for the muscle isoform (74°) but not the liver isoform (45°) (27–29) (Fig. 5, *c* and *d*). The tower helices in all three isozymes are stabilized by non-polar interactions between Val^{266}, Leu^{267}, and Asn^{270} and their counterparts from the other subunit (Fig. 5, *b*–*d*). However, in contrast to mGP and lGP, the two tower helices from bGP also interact through two additional hydrogen bonds: one between the lateral side chains of Tyr^{262} and $Asn^{270\prime}$ at one end of the helical interface and the other between Asn^{270} and $Tyr^{262\prime}$ at the other end (Fig. 5*b*). Moreover, whereas lGP has a rigid structure (27, 29) and little remodeling occurs during the activation process, mGP displays a flexible functional dimer interface, which is remodeled upon activation. In both bGP structures, the functional dimer interface has a buried surface of 1400 $Å^2$, whereas the buried surface of the functional dimer interface of mGP is of 2240 $Å^2$. This is consistent with a flexible functional dimer interface and the similar regulatory features shared between muscle and brain GP.

The Packing Dimer Interface and the Tetramer Interface of bGP—Interaction between the two functional bGP dimers relies on contacts involving the tower helices, the glycogen storage site (residues 426–434), and the bundle of helices α26 to 29 (residues 721–769), as previously described for the muscle isozyme (33). No tetrameric structure has been observed for lGP, and thus, such an interface does not exist (29) (Fig. 6*a*). The bGP and AMP-bound bGP structures display a similar packing dimer interface, although there are a few more contacts involving the glycogen storage site in the bGP tetramer without AMP (data not shown).

The tower helices in bGP constitute a substantial part of the interactions established at the packing dimer interface, further stabilizing this interaction, contrary to the muscle isoform (33). Indeed, the N-terminal extremity of the tower helices in bGP allow the formation of hydrophobic contacts between Val^{259}, Tyr^{262}, Ile^{263}, and their relative symmetric equivalents. The gate from each subunit is stabilized in the open conformation through hydrophobic contacts between Phe^{286} and Asn^{281}, and their symmetric equivalents (Fig. 6*b*). Nevertheless, the number of contacts slightly decreases in the presence of the allosteric effector, affecting mostly in the glycogen storage site. Indeed, in this site, half of the contacts are lost (data not shown).

The Core of Tower Helices—The tower helices of bGP constitute the core of the tetramer interface as they do in mGP (33). The tower helices of AMP-bound bGP are longer by two turns than in AMP-bound mGP (28), allowing each tower helix to interact with the helices from the three other subunits.

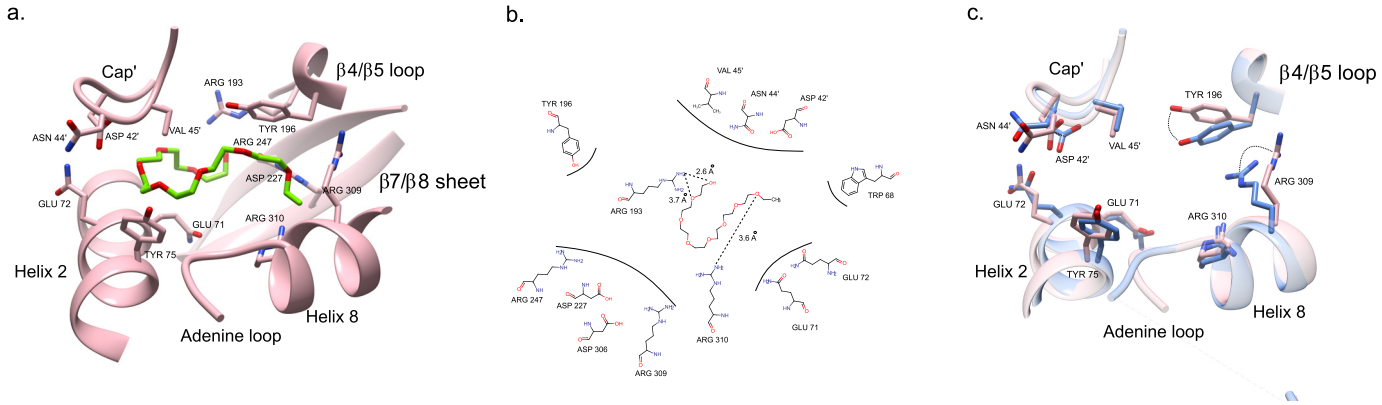

FIGURE 4. **Presence of PEG 400 in AMP binding site.** *a*, PEG 400 is localized to the AMP binding. The Cα trace of the main regions implicated in PEG 400 stabilization is represented as a *ribbon*. The amino acids interacting with PEG 400 are shown and labeled. *b*, plot diagram of the interactions of PEG400 with the residues from the bGP AMP-binding site. Hydrogen bonds are shown as *dashed lines*. Additional van der Waals contacts are represented as *black curved lines*. Most of the residues implicated in the stabilization of PEG 400 are also involved in the binding of AMP. *c*, overlay of the AMP-binding sites of the two bGP structures: bGP in complex with PEG 400 in *pink*; bGP in complex with AMP in *blue*. Residues that undergo reorientation following the binding of AMP are represented.

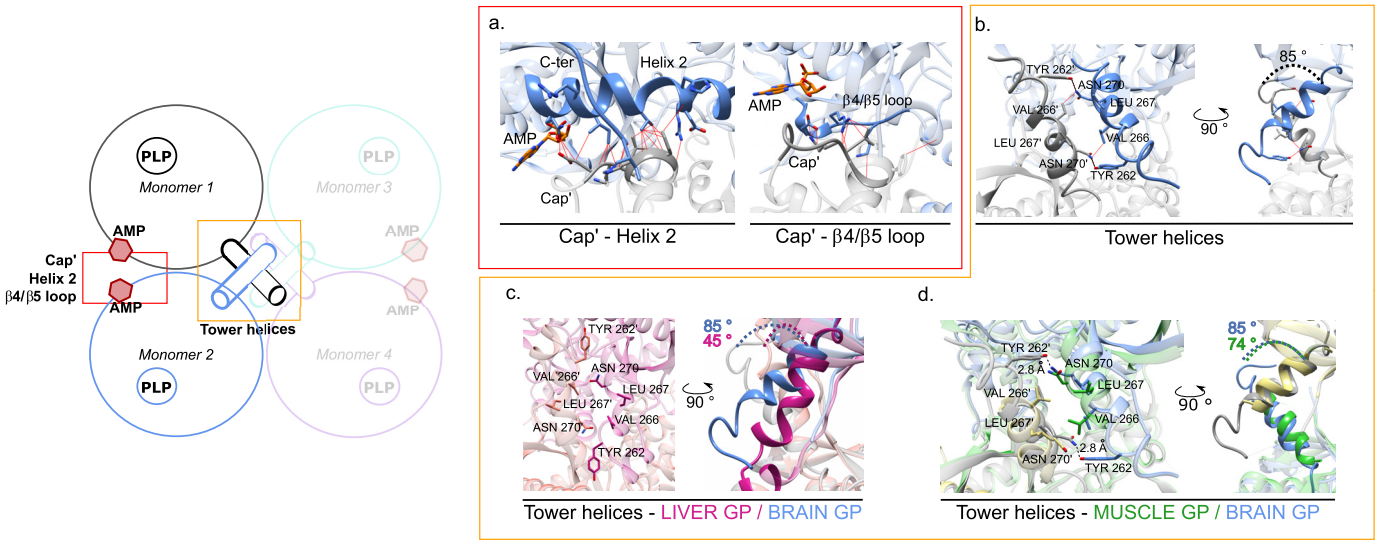

FIGURE 5. **The functional dimer interface.** Ribbon representations of the regions involved in the functional dimer interface of bGP are shown. The regions described are indicated, and the residues making contacts at the interface are represented and labeled. A schematic representation of the tetramer is shown (*left panel*), highlighting the interface we describe below. *a*, the functional dimer interface of bGP involves the helix 2-cap′ loop-β4/β5 loop region, comprising the AMP-binding site, and the tower helices. *b*, *first panel*, the tower helix of bGP from one monomer (*blue*) interacts with its counterpart (*gray*) forming hydrogen bonds and hydrophobic contacts. *Second panel*, interactions at the interface promote the arrangement of the tower helices by a crossover angle of 85°. *c*, overlay of the crystal structure of the tower helices interface of lGP (1 FA9; *dark* and *light pink*) and bGP (*blue* and *gray*). Active conformation (R state) of lGP is characterized by a 45° crossover angle of the tower helices and hydrophobic contacts between Val^{266}, Leu^{267}, and Asn^{270} and their equivalents on the other subunit. *d*, overlay of the crystal structures of the tower helices interface of the active R state of mGP (1PYG; *green* and *beige*) and bGP (*blue* and *gray*). The mGP tower helices interact solely through hydrophobic contacts involving Val^{266}, Leu^{267}, and Asn^{270} and their equivalents on the other subunit, similar to lGP. These interactions stabilize the tower helices in the active conformation, displaying a crossover angle of 74°.

Opposite subunits from the tetramer (for example monomers 1 and 4) are thus able to interact through the tower helices via the establishment of non-polar interactions between Leu^{271} and $Gly^{260\prime}$, as well as Leu^{268} and $Ile^{263\prime}$, on one side, and their relative counterparts $Leu^{271\prime}$, Gly^{260}, $Leu^{267\prime}$, and Ile^{263}, on the other (Fig. 6*c*). Although the tower helices contribute to less than 10% of the total interactions in the active muscle tetramer, they contribute to a fourth of the total contacts found in the whole tetramer in the PEG-bound bGP structure. In AMP-bound bGP, more than half of these contacts are lost. This leads to a reduction of the packing of the core formed by the tower helices, helix 8, and the gate, thus relaxing the tetramer interface (data not shown).

The AMP-binding Site—The AMP-binding site of bGP is delimited by the cap′ loop from one subunit and helix 2, helix 8, and the β4/β5 loop from the other subunit, because they are in the muscle and liver isoforms (27–29). Helix 2 extends across the width of the protein and ensures the connection between the two AMP-binding sites of the functional dimer (Figs. 2*c* and 7*a*). Side chains of the residues involved in the binding of AMP move to improve their contacts with AMP in the AMP-bound bGP structure (Fig. 4*c*). The AMP-binding site can be divided into three subsites: one each for the phosphate, sugar, and base moiety of AMP (1, 27, 28). The phosphate group of AMP interacts with the AMP-binding site in the AMP-bound structure of bGP by forming several hydrogen bonds involving the side

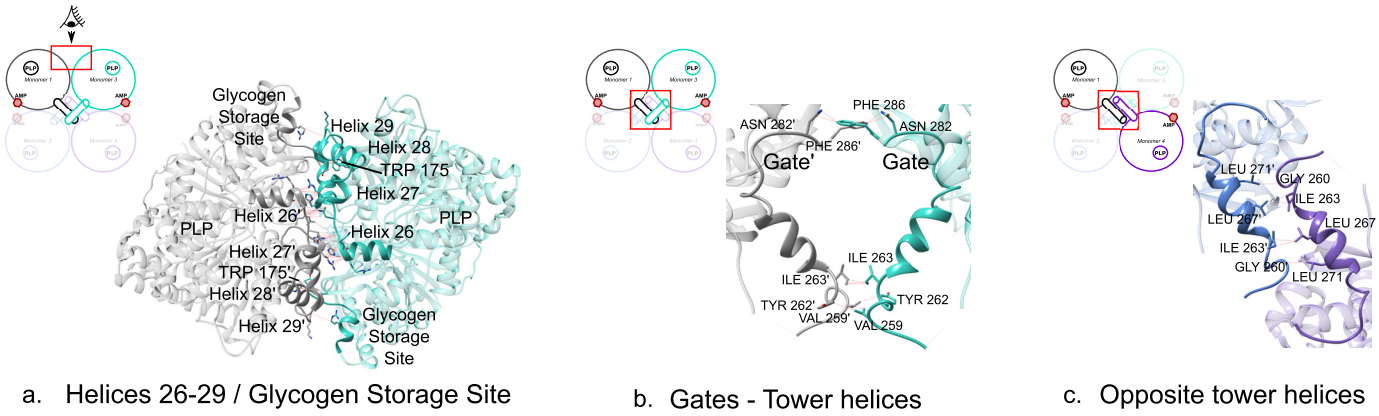

FIGURE 6. **The tetramer interfaces.** Ribbon representations of the regions involved in the tetramer interfaces in AMP-bound bGP are shown. The described regions are indicated, and the residues involved in the interactions are represented and labeled. *a*, the packing dimers interact through contacts involving the bundle of loops and helices 26–29, as well as the glycogen storage site. *b*, the tower helices interactions at the packing dimer interface. Tower helices interact through Val^{259}, Tyr^{262}, and Ile^{263} and stabilize the gate loop in the open configuration. *c*, interactions between the tower helices from two opposite subunits. The tower helices from two opposite subunits from the bGP tetramer interact through hydrophobic contacts.

chains of Arg^{309} and Arg^{310} from helix 8 and the side chain of Tyr^{196} from the $\beta4/\beta5$ loop (Figs. 7*a* and 8*a*). The ribose of AMP interacts with the cap′ loop, forming a hydrogen bond with $Asp^{42'}$ and van der Waals contacts with $Asn^{44'}$ and $Val^{45'}$. The nucleotide moiety of AMP interacts weakly with helix 2, forming van der Waals interactions with the side chains of Gln^{71} and Gln^{72}, and co-planar stacking with the side chain of Tyr^{75} (Figs. 7*b* and 8*a*). All these interactions may contribute to a 24° rotation of the nucleotide moiety of AMP relative to AMP-bound mGP (Fig. 7*b*). The activation of mGP by AMP and its cooperative binding are partly attributed to the formation of several hydrogen bonds with the AMP-binding site and its further stabilization in the AMP-binding site by the adenine loop (residues 312–325) (27–29) (Fig. 7*b* and 8*a*). In contrast, the liver isoform interacts poorly with AMP, consistent with its weak activation by AMP (29) (Fig. 8*a*). Surprisingly, we did not observe electron density for the adenine loop in both structures (the PEG-bound and AMP-bound bGP structures) (Fig. 8*b*), despite the high sensitivity of bGP to AMP-dependent activation and the sequence conservation between the muscle and brain isoforms. The side chain of Tyr^{75} adopts a conformation that precludes the interaction of the adenine loop (312–325) with AMP, as for lGP (29) (Fig. 7*b*). The conformation of Tyr^{75} in bGP is stabilized by the formation of a hydrogen bond between the phosphate group of AMP and Tyr^{196}, a residue only found in the brain isozyme (corresponding to Phe^{196} in muscle and liver GP). This unique interaction thus contributes to the geometry of AMP in bGP and by favoring the co-planar stacking between Tyr^{75} and the nucleotide part of AMP (Fig. 7*c*).

Discussion

Brain glycogen provides fuel for neuronal and astrocyte functions. It is critical for high cognitive processes including learning and memory consolidation (10–17). In humans, glycogen phosphorylase, the key enzyme for glycogen mobilization, consists of three isozymes, including one specific for brain. Whereas the structures of mGP and lGP have been known for decades, the structure of bGP is still lacking despite its critical role in brain glycogen metabolism (25, 26, 29).

We report the first crystal structure of human bGP. We found the overall crystal structure of bGP is similar to lGP and mGP, consistent with the sequence conservation of GP isozymes (83 and 80% sequence identity of bGP with the muscle and liver GP, respectively). GP isozymes differ in their responses to allosteric activation, in particular to AMP, despite their structural similarity. The liver isozyme is mostly controlled by phosphorylation, whereas the muscle and brain isozymes are strongly activated by AMP activation (1, 23, 24). These observations are consistent with our findings; the structure of the AMP-bound bGP (active form) is more closely related to active mGP than active lGP, especially concerning the tower helices interface and the overall relationship between the two monomers of the functional dimers. These features suggest that the activation process of bGP relies on the remodeling of the functional dimer interface, as for mGP (27, 28). In contrast, lGP has a more rigid structure, and no such remodeling occurs upon activation (29). This is further supported by the buried surface of the functional dimer interface of lGP (3350 $Å^2$) relative to the two other GP isozymes (2240 $Å^2$ for mGP and 1400 $Å^2$ for bGP). However, bGP and mGP also demonstrate distinct regulatory features (23, 24).

Although the phosphorylation peptide (1–21) is stabilized and seen in structures of AMP-bound mGP, no electron density was obtained for this region in AMP-bound bGP (Fig. 2, *a* and *c*). It is possible that differences in flexibility/dynamics of this region (which is not fully conserved between the three isoforms) may explain the lower sensitivity of bGP to activation by phosphorylation (23).

Whereas mGP responds cooperatively to activation by AMP, bGP is activated noncooperatively by AMP (23). The AMP-bound bGP structure shows that AMP forms several hydrogen bonds within the AMP binding site (Figs. 7 and 8) as observed for AMP-bound mGP but not AMP-bound lGP. However, as observed for lGP, we found that helix 2 of bGP interacts poorly with AMP (no hydrogen bond) and that Tyr^{75} adopts a conformation that may preclude the stabilization of the adenine loop (which is not observed in our structure because of a lack of electron density) (Fig. 7). These features have also been put

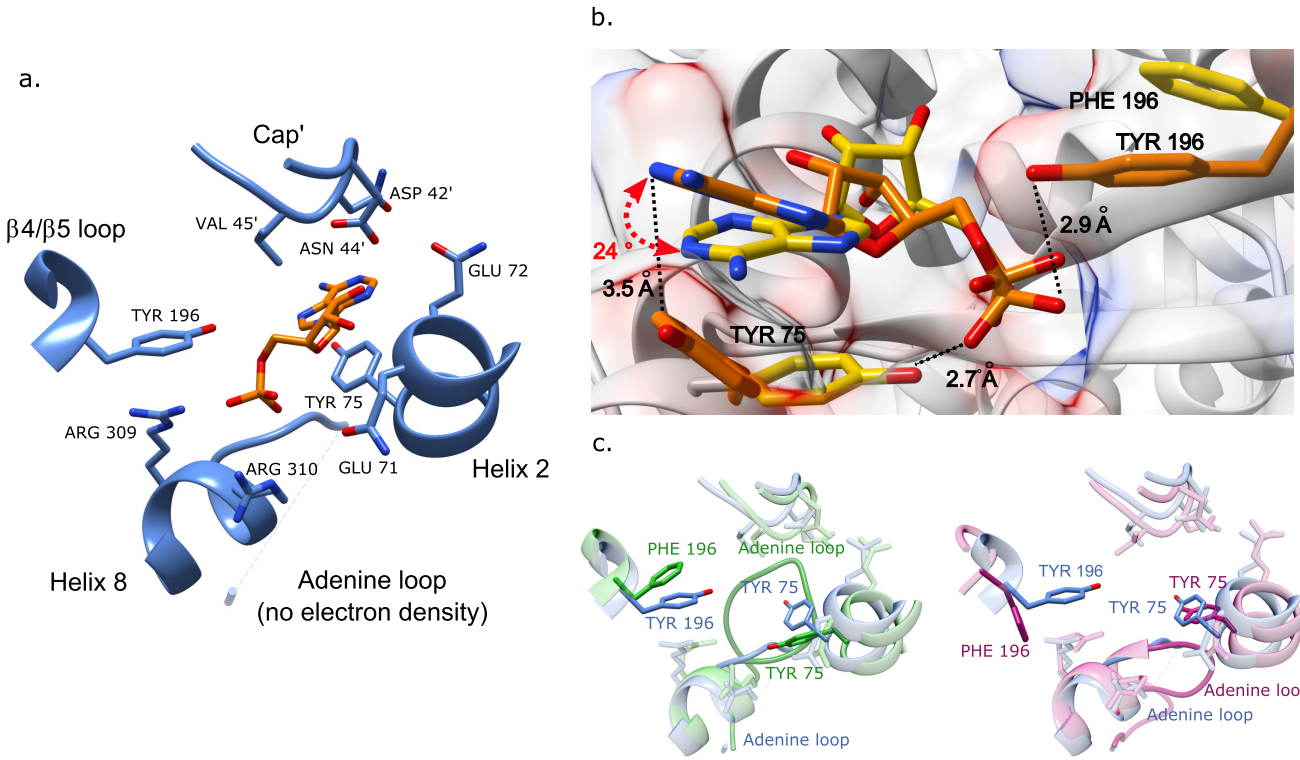

FIGURE 7. **The AMP-binding site of human bGP.** *a*, the binding mode of AMP in the bGP AMP-binding site. The AMP-binding site corresponds to a cleft formed by helix 2, helix 8, β4/β5, and the cap′ loop. The main regions implicated in AMP binding are represented as *blue ribbons*. Residues interacting with AMP are shown and labeled. No electron density was observed for the adenine loop, despite AMP binding. *b*, superposition of the crystal structure of AMP in the mGP (*yellow*) and bGP (*orange*) AMP-binding sites. The conformation of AMP in the AMP-binding site of bGP differs from that of mGP. *c*, overlay views of the AMP-binding site of bGP, mGP (1PYG), and lGP (1FA9). The main regions of bGP depicted in Fig. 6*a* (*blue*) are aligned with the corresponding regions in mGP (*green*) and lGP (*pink*). The AMP located in the AMP-binding site is not displayed for clarity. The replacement of Phe[196] of muscle and liver GP by a tyrosine residue in bGP allows this amino acid to interact with the AMP. The Tyr[75] avoids the stabilization of the adenine loop in lGP and bGP.

forward to explain the absence of cooperative binding of AMP to lGP (29). We also found that Tyr[196] in bGP, located at the functional dimer interface (equivalent to Phe[196] in mGP and lGP), makes a hydrogen bond with AMP that is specific for bGP (Figs. 7 and 8). Interestingly, this bGP specific substitution (F196Y) has been suggested to alter AMP cooperativity (23).

The conformation of the adenine loop is known to play a role in AMP binding and activation. The adenine loop is well defined in the AMP-bound mGP structures, whereas it is poorly ordered in AMP-bound lGP and not observed in AMP-bound bGP (no electron density) (28, 29). Altogether, these observations may explain the non-cooperative binding of AMP to bGP upon AMP activation.

bGP is critical for the support of brain processes because it allows the mobilization of the brain glycogen store (10–17). The importance of bGP is further supported by the fact that no mutations for this isozyme have been reported. Indeed, whereas deleterious mutations of the liver and muscle isozymes lead to the development of glycogen storage diseases (Hers disease and McArdle disease, respectively), no deleterious mutations are known for bGP (1). This is likely because bGP is the only GP isozyme expressed during fetal development and is later replaced by mGP and lGP in their respective organs. It is likely that altered bGP activity is lethal during early embryonic development (1). The co-expression of the brain and muscle isoforms in astrocytes further underlines the functional importance of the brain isozyme for neuronal processes (34). Indeed it has been shown that whereas mGP rapidly responds to extracellular signals in brain such as noradrenaline, bGP is critical for local energy metabolism via changes in AMP concentration (23, 24). The distinct regulatory features of brain and muscle GP, in particular the cooperative and non-cooperative binding of AMP, allow astrocytes to tightly adapt their responses to their energy needs. Moreover, it is now accepted that the accumulation of glycogen in neurons leads to their rapid degeneration and is implicated in aging, as well as promoting several pathological conditions of the brain such as Lafora disease. The activity of bGP is critical for the controlled degradation of glycogen in neurons because they only express the brain isoform of GP (17). A reduction of bGP activity would lead to the uncontrolled accumulation of glycogen in neurons and contribute to the pathogenesis of several brain diseases (18, 35, 36).

In conclusion, the crystal structures of human bGP reported in this study contribute to a better understanding of this specific isozyme and a deeper knowledge of the differences in the activation properties of this important family of allosteric enzymes. Additionally, these new structural insights may enable isozyme-specific rational drug design for therapeutic development (37–39).

Experimental Procedures

Materials—Antibodies raised against brain glycogen phosphorylase were obtained from Santa Cruz (SC-81751). Anti-phosphoserine and anti-histidine tag antibodies, L-arabinose,

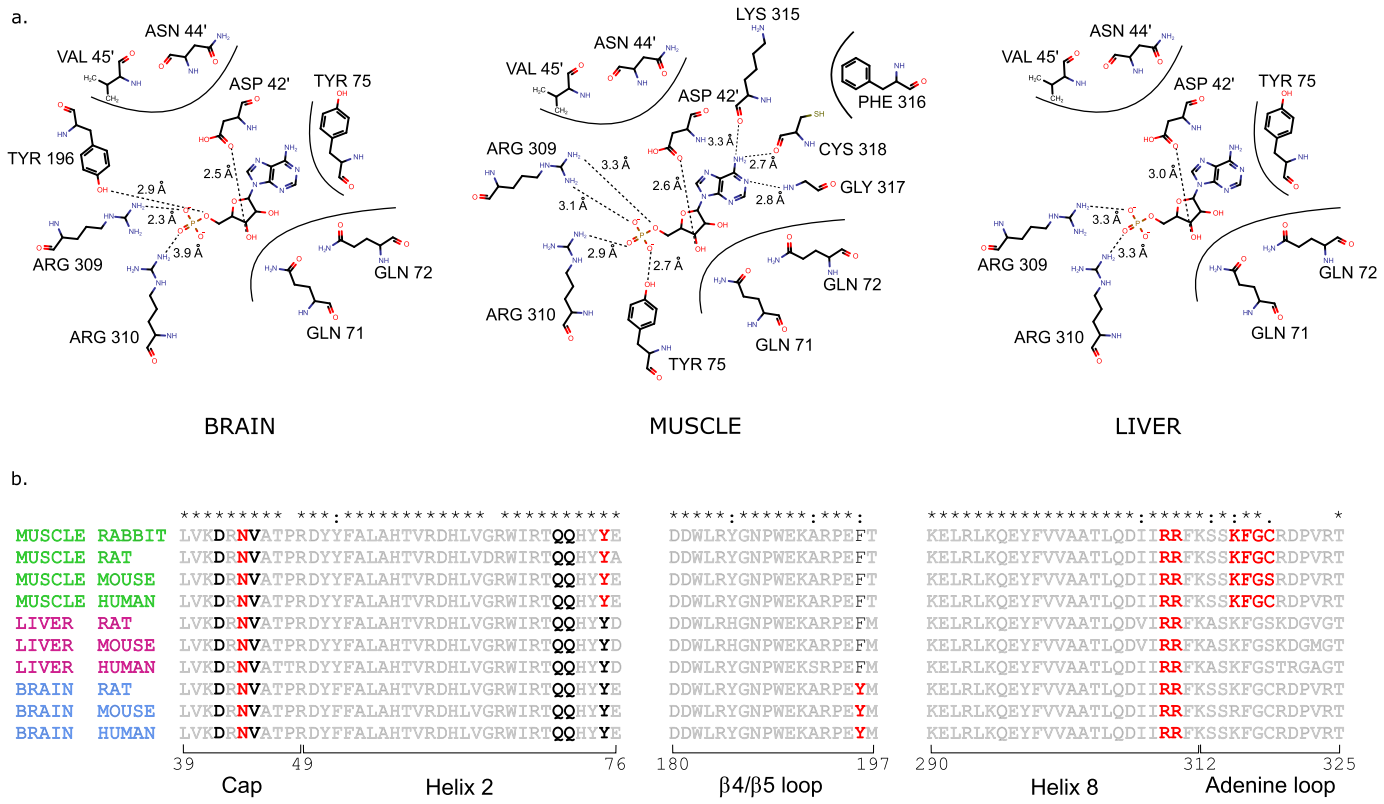

FIGURE 8. **Residues involved in the binding of AMP.** *a*, sequence alignment of the regions involved in the binding of AMP in GPs. Residues involved in the binding of AMP are in *bold*. Residues involved in hydrogen bonds with AMP are shown in *red*, and residues establishing van der Waals interactions with AMP are shown in *black*. Sequences are highly conserved between the different isoforms, except for the liver isoform adenine loop. *b*, interaction plot diagram of AMP with the AMP-binding site residues from brain, muscle, and liver GP. Hydrogen bonds are shown as *dashed lines*. Additional van der Waals contacts are represented as *black curved lines*. Whereas Tyr^{75} and residues of the adenine loop forms hydrogen bonds with AMP in mGP, no such interactions are observed for lGP and bGP.

protease inhibitor mixture, nickel-nitrilotriacetic acid Superflow resin, bovine serum albumin, imidazole, streptavidin-agarose resin, phosphoglucomutase, EDTA, glucose-1,6-diphosphate, AMP, ATP, phosphorylase kinase from rabbit muscle, BSA, and glycogen were purchased from Sigma-Aldrich. Glucose-6-phosphate dehydrogenase was purchased from Roche. ECL Western blotting detection reagent was purchased from GE Heathcare. Biotinylated thrombin was purchased from Merck Millipore. NADP was purchased from Apollo Scientific.

Cloning of bGP and Expression of Recombinant bGP—The human bGP cDNA (provided by OriGene Technologies, Inc.) was subcloned into the pET28a vector for further expression of His_6-tagged fusion recombinant proteins (6xHis-bGP). *E. coli* C41(DE3)/pGro7 (encoding the GroEL-GroES chaperonin protein complex) strains were transformed with plasmid pET28a carrying 6xHis-bGP and used to express and purify the recombinant protein. Expression of the GroEL-GroES chaperonin protein complex was first induced by the addition of 1 mM L-arabinose to cultures at an A_{600} value of 0.2–0.3. Expression of recombinant bGP was then induced by the addition of 500 μM of isopropyl-1-thio-β-D-galactopyranoside to cultures at an A_{600} value of 0.6–0.8. The bacteria were further cultured at 16 °C overnight. The bacteria were pelleted by centrifugation (4,000 × *g*, 10 min), washed with cold PBS, and harvested by centrifugation (4,000 × *g*, 10 min). The pellets were stored at −80 °C until required.

Purification of Recombinant bGP from E. coli—Extraction and purification were repeatedly performed to obtain 20 mg of protein. The bacteria were resuspended in 35 ml of lysis buffer (PBS, pH 8, 300 mM NaCl, 0.5% Triton X-100, 1 mg/ml lysozyme, protease inhibitor mixture (Sigma-Aldrich)) and incubated for 1 h at 4 °C. The lysate was sonicated on ice (8-s pulses for up to 7 min) and centrifuged (17,000 × *g*, 30 min, 4 °C). The supernatant was collected and incubated with 1 ml of nickel-nitrilotriacetic acid Superflow resin (Sigma-Aldrich) in the presence of 10 mM imidazole (final concentration) for a minimum of 2 h at 4 °C. The resin was then poured into a column and washed successively with washing buffer (PBS, pH 8, 300 mM NaCl) containing 0.1% Triton X-100 and a stepwise gradient of imidazole in washing buffer until a concentration of 20 mM imidazole (final concentration) was achieved. His-tagged proteins were eluted with washing buffer containing 300 mM imidazole. Purified proteins were then incubated for 10 min with 10 mM DTT and protease inhibitor mixture. The purified protein was then exchanged against PBS, pH 7.1, using a PD10 (GE Healthcare) desalting column. The protein concentration was measured using the standard Bradford assay with BSA as standard and by absorbance measurement at 280 nm using a theoretical ϵ_M: 115170 M^{-1} cm^{-1}. The purity of the protein was assessed by SDS-PAGE analysis.

His_6 Tag Cleavage by Thrombin Digestion—The His_6 tag was removed by thrombin digestion. Briefly, 20 mg of 6xHis-bGP

was incubated with biotinylated-thrombin (0.5 units thrombin/mg protein, purchased from Merck-Millipore) for 3 h on ice. Biotinylated thrombin was removed from the mixture by the addition of streptavidin-agarose resin (16 μl/unit thrombin, Sigma-Aldrich) for 30 min at 4 °C with agitation. The resin was collected by centrifugation (10 min at 1,000 × *g*). The supernatant was collected and centrifuged on a Vivaspin 12 MWO (GE Heathcare) to remove the His tag fragment and to concentrate the bGP. The proteins were then subjected to buffer exchange against 20 mM Tris-HCl, pH 6.9, using a PD10 buffer exchange column (GE Healthcare) and concentrated to a concentration of 7 mg/ml.

Enzyme Assay—bGP activity was measured in the direction of glycogenolysis as described elsewhere (40). Briefly, the formation of glucose-1-phosphate was determined using a coupled assay system containing phosphoglucomutase, glucose-6-phosphate dehydrogenase, and NADP, by following $NADPH,H^+$ formation at 340 nm. The phosphorylase activity assay was carried out at 37 °C in PBS, pH 6.9. The mixture consisted of bGP (final concentration, 0.1 μM) with or without 1 mM AMP, 0.25% glycogen, 2 mM EDTA, 0.8 mM NADP, 10 mM magnesium acetate, 5 μM glucose-1,6-diphosphate, 5 units of glucose-6-phosphate dehydrogenase, and 5 units phosphoglucomutase, in a final volume of 250 μl. Each measurement was performed in triplicate.

Biochemical Analysis of Recombinant bGP—The saturation curve by glycogen was obtained by measuring the bGP activity with various concentrations of glycogen (0–0.35%) in the presence of a saturating concentration of AMP (1 mM). The level of activation of bGP by the allosteric activator AMP was obtained by measuring bGP activity in the presence of a saturating concentration of glycogen (0.025%) and various concentrations of AMP (0–3 mM). Initial velocities were determined, and cooperativity of AMP binding was assessed by fitting the data to the Hill equation,

$$\mathrm{Log}(Y/(1-Y)) = n\mathrm{log}[\mathrm{AMP}] - \mathrm{log}K_A \qquad \text{(Eq. 1)}$$

where Y is the ratio V_i/V_{max}, n is the Hill coefficient, [AMP] is the corresponding concentration of AMP, and K_A is the affinity constant.

Phosphorylation of Ser^{14} and Activation by Phosphorylation—bGP was phosphorylated using phosphorylase kinase from rabbit muscle (Sigma-Aldrich) (1 unit/mg bGP) activated by preincubation for 1 h in phosphorylation buffer containing 20 mM Tris-HCl buffer, pH 7.7, 0.22 mM ATP, 3.3 mM $MgCl_2$, 0.5 mM $CaCl_2$, 0.5 mM NaF for activation. Phosphorylation was performed by the addition of activated phosphorylase kinase to the bGP solution and in phosphorylation buffer and incubation for 2 h at room temperature. The resulting activity was assessed with or without AMP. Phosphorylation of rabbit mGP (Sigma-Aldrich) was used as a control. Phosphorylated bGP was then subjected to buffer exchange against PBS buffer, pH 6.9, using a PD Minitrap G25 (GE Healthcare) desalting column.

SDS-PAGE Electrophoresis and Western Blotting—Proteins were loaded onto 7.5% polyacrylamide gels and electrophoretic protein separation carried out at 110 V (constant voltage). For SDS-PAGE, the presence of proteins was revealed using R-250 Coomassie Blue. After migration by SDS-PAGE, the proteins were transferred onto a nitrocellulose membrane at a constant current of 200 mA at 4 °C for 1 h. Membranes were incubated at 4 °C overnight with appropriately diluted primary antibody. After washing, the membranes were incubated for 2 h at room temperature with peroxidase-coupled secondary antibody. The proteins were visualized by chemiluminescence detection using ECL substrate (GE Healthcare) and LAS 4000 (Fuijifilm).

Native Mass Spectrometry—bGP was purified, and the His tag was removed as described above. Native MS was performed on samples containing bGP (1 mg/ml) and phosphorylated bGP (1 mg/ml) using an Exactive Plus EMR mass spectrometer (Thermo Fisher Scientific), which allows analysis of proteins and complexes in native-like states (41). The proteins were desalted by buffer exchange prior to mass spectrometry analysis.

Dynamic Light Scattering Measurements—Dynamic light scattering measurements were performed with a DynaPro-MS800 molecular sizing instrument (Protein Solutions, Lakewood, NJ). Protein samples at 3.2 mg/ml in 20 mM Tris-HCl, pH 7.0, in the presence or in the absence of 5 mM AMP were loaded into a 45-μl quartz cuvette. The hydrodynamic radius and molecular mass were determined from 50 measurements at 18 °C. The data were analyzed using Dynamics 6.9.2.11 software.

Crystallization of bGP and Soaking with AMP—Initial screening of crystallization conditions was carried out by the vapor diffusion method using a Mosquito^{TM} nanoliter-dispensing system (TTP Labtech) at 4 °C. Sitting drops were set up using 400 nl of a 1:1 mixture of recombinant human bGP at 7 mg/ml and crystallization solutions (672 different commercially available conditions) equilibrated against a 150-μl reservoir in multiwell plates (Greiner Bio-One). The crystallization plates were stored at 4 °C in a RockImager1000^{TM} (Formulatrix) automated imaging system to monitor crystal growth. Hits were improved by making handmade hanging drops in 24-well plates at 18 °C. The best crystals were obtained using a solution of 28% (v/v) PEG 400, 0.2 M calcium chloride, and 0.1 M Hepes, pH 7.5. Crystals with dimensions of up to 0.05 mm × 0.05 mm × 0.1 mm appeared within 2 weeks. The crystal of protein complexed with AMP (AMP-bound bGP) was obtained by soaking the apo-form crystal for 3 h in 50 mM of AMP dissolved into the crystallization solution. For data collection, the crystals were flash-cooled in liquid nitrogen using the mother crystallization solution as cryoprotectant. All x-ray diffraction data were collected on the PROXIMA-1 Beamline at the Soleil Synchrotron (St. Aubin, France) and the ID23-2 at European Synchrotron Radiation Facility (Grenoble, France). Diffraction images were integrated using the XDS program (42).

Structure Determination, Refinement, and Analysis—For the resolution of the structure, molecular replacement phases were obtained using Phaser (43) implemented in the CCP4 program suite (Collaborative Computational Project, Number 4 (44)). The model for molecular replacement was built by homology modeling using SWISS-MODEL (45) based on the template structure of human muscle glycogen phosphorylase (PDB code 1Z8D). The initial models were completed and adjusted using the COOT program (46). Refinement was performed using REFMAC as implemented in CCP4 (47). The crystal structure of the PEG-

bound GPb at 2.5 Å resolution was refined to R and R_{free} crystallographic factors of 18 and 24%, respectively (see statistics in Table 1). The crystal structure of the AMP-bound bGP at 3.4 Å resolution was refined to R and R_{free} crystallographic factors of 21 and 29%, respectively (see statistics in Table 1). Atomic coordinates and structure factors were deposited in the Protein Data Bank under accession codes 5IKO and 5IKP for the PEG-bound GPb and the AMP-bound bGP, respectively.

Molecular Graphics and Analyses—Molecular graphics and analyses were performed using the UCSF Chimera package (1.10.2). Chimera was developed by the Resource for Biocomputing, Visualization, and Informatics at the University of California, San Francisco (UCSF Chimera-a visualization system for exploratory research and analysis (48)).

Author Contributions—C. M. and F. R.-L. designed experiments, managed the project, and wrote the manuscript. C. M., I. L. S.-G., R. D., X. X., A. C., T. L., G. W., J.-M. C., C. E., A. H., J.-M. D., and F. R.-L. performed experiments and/or analyzed the data. All authors discussed the results and commented on the manuscript.

Acknowledgments—We acknowledge SOLEIL and ESRF for provision of synchrotron radiation facilities, and we thank the staff for assistance in using beamline PROXIMA1 and ID23–1, respectively.

References

1. Newgard, C. B., Hwang, P. K., and Fletterick, R. J. (1989) The family of glycogen phosphorylases: structure and function. *Crit. Rev. Biochem. Mol. Biol.* **24,** 69–99
2. Berg, J. M., Tymoczko, J. L., Stryer, L., and Clarke, N. D. (2002) *Biochemistry*, 5th ed., pp 831–863, W. H. Freeman, New York
3. Öz, G., DiNuzzo, M., Kumar, A., Moheet, A., and Seaquist, E. R. (2015) Revisiting glycogen content in the human brain. *Neurochem. Res.* **40,** 2473–2481
4. Obel, L. F., Müller, M. S., Walls, A. B., Sickmann, H. M., Bak, L. K., Waagepetersen, H. S., and Schousboe, A. (2012) Brain glycogen-new perspectives on its metabolic function and regulation at the subcellular level. *Front. Neuroenergetics.* **4,** 3
5. Brown, A. M. (2004) Brain glycogen re-awakened. *J. Neurochem.* **89,** 537–552
6. Hossain, M. I., Roulston, C. L., and Stapleton, D. I. (2014) Molecular basis of impaired glycogen metabolism during ischemic stroke and hypoxia. *PLoS One* **9,** e97570
7. Choi, I.-Y., Seaquist, E. R., and Gruetter, R. (2003) Effect of hypoglycemia on brain glycogen metabolism *in vivo*. *J. Neurosci. Res.* **72,** 25–32
8. Suh, S. W., Bergher, J. P., Anderson, C. M., Treadway, J. L., Fosgerau, K., and Swanson, R. A. (2007) Astrocyte glycogen sustains neuronal activity during hypoglycemia: studies with the glycogen phosphorylase inhibitor CP-316,819 ([R-R*,S*]-5-chloro-*N*-[2-hydroxy-3-(methoxymethylamino)-3-oxo-1-(phenylmethyl)propyl]-1H-indole-2-carboxamide). *J. Pharmacol. Exp. Ther.* **321,** 45–50
9. Swanson, R. A., Sagar, S. M., and Sharp, F. R. (1989) Regional brain glycogen stores and metabolism during complete global ischaemia. *Neurol. Res.* **11,** 24–28
10. Suzuki, A., Stern, S. A., Bozdagi, O., Huntley, G. W., Walker, R. H., Magistretti, P. J., and Alberini, C. M. (2011) Astrocyte-neuron lactate transport is required for long-term memory formation. *Cell* **144,** 810–823
11. Newman, L. A., Korol, D. L., and Gold, P. E. (2011) Lactate produced by glycogenolysis in astrocytes regulates memory processing. *PLoS One* **6,** e28427
12. Pellerin, L., and Magistretti, P. J. (2012) Sweet sixteen for ANLS. *J. Cereb. Blood Flow Metab.* **32,** 1152–1166
13. Gibbs, M. E., Anderson, D. G., and Hertz, L. (2006) Inhibition of glycogenolysis in astrocytes interrupts memory consolidation in young chickens. *Glia* **54,** 214–222
14. Gibbs, M. E., and Hutchinson, D. S. (2012) Rapid turnover of glycogen in memory formation. *Neurochem. Res.* **37,** 2456–2463
15. Duran, J., Saez, I., Gruart, A., Guinovart, J. J., and Delgado-García, J. M. (2013) Impairment in long-term memory formation and learning-dependent synaptic plasticity in mice lacking glycogen synthase in the brain. *J. Cereb. Blood Flow Metab.* **33,** 550–556
16. Duran, J., and Guinovart, J. J. (2015) Brain glycogen in health and disease. *Mol. Aspects Med.* **46,** 70–77
17. Saez, I., Duran, J., Sinadinos, C., Beltran, A., Yanes, O., Tevy, M. F., Martínez-Pons, C., Milán, M., and Guinovart, J. J. (2014) Neurons have an active glycogen metabolism that contributes to tolerance to hypoxia. *J. Cereb. Blood Flow Metab.* **34,** 945–955
18. Vilchez, D., Ros, S., Cifuentes, D., Pujadas, L., Vallès, J., García-Fojeda, B., Criado-García, O., Fernández-Sánchez, E., Medraño-Fernández, I., Domínguez, J., García-Rocha, M., Soriano, E., Rodríguez de Córdoba, S., and Guinovart, J. J. (2007) Mechanism suppressing glycogen synthesis in neurons and its demise in progressive myoclonus epilepsy. *Nat. Neurosci.* **10,** 1407–1413
19. Duran, J., Tevy, M. F., Garcia-Rocha, M., Calbó, J., Milán, M., and Guinovart, J. J. (2012) Deleterious effects of neuronal accumulation of glycogen in flies and mice. *EMBO Mol. Med.* **4,** 719–729
20. Lebo, R. V., Gorin, F., Fletterick, R. J., Kao, F. T., Cheung, M. C., Bruce, B. D., and Kan, Y. W. (1984) High-resolution chromosome sorting and DNA spot-blot analysis assign McArdle's syndrome to chromosome 11. *Science* **225,** 57–59
21. Newgard, C. B., Fletterick, R. J., Anderson, L. A., and Lebo, R. V. (1987) The polymorphic locus for glycogen storage disease VI (liver glycogen phosphorylase) maps to chromosome 14. *Am. J. Hum. Genet.* **40,** 351–364
22. Newgard, C. B., Littman, D. R., van Genderen, C., Smith, M., and Fletterick, R. J. (1988) Human brain glycogen phosphorylase. Cloning, sequence analysis, chromosomal mapping, tissue expression, and comparison with the human liver and muscle isozymes. *J. Biol. Chem.* **263,** 3850–3857
23. Crerar, M. M., Karlsson, O., Fletterick, R. J., and Hwang, P. K. (1995) Chimeric muscle and brain glycogen phosphorylases define protein domains governing isozyme-specific responses to allosteric activation. *J. Biol. Chem.* **270,** 13748–13756
24. Müller, M. S., Pedersen, S. E., Walls, A. B., Waagepetersen, H. S., and Bak, L. K. (2015) Isoform-selective regulation of glycogen phosphorylase by energy deprivation and phosphorylation in astrocytes. *Glia* **63,** 154–162
25. Fletterick, R. J., Sygusch, J., Semple, H., and Madsen, N. B. (1976) Structure of glycogen phosphorylase a at 3.0 A resolution and its ligand binding sites at 6 A. *J. Biol. Chem.* **251,** 6142–6146
26. Barford, D., Hu, S. H., and Johnson, L. N. (1991) Structural mechanism for glycogen phosphorylase control by phosphorylation and AMP. *J. Mol. Biol.* **218,** 233–260
27. Barford, D., and Johnson, L. N. (1989) The allosteric transition of glycogen phosphorylase. *Nature* **340,** 609–616
28. Sprang, S. R., Withers, S. G., Goldsmith, E. J., Fletterick, R. J., and Madsen, N. B. (1991) Structural basis for the activation of glycogen phosphorylase b by adenosine monophosphate. *Science* **254,** 1367–1371
29. Rath, V. L., Ammirati, M., LeMotte, P. K., Fennell, K. F., Mansour, M. N., Danley, D. E., Hynes, T. R., Schulte, G. K., Wasilko, D. J., and Pandit, J. (2000) Activation of human liver glycogen phosphorylase by alteration of the secondary structure and packing of the catalytic core. *Mol. Cell* **6,** 139–148
30. Gaboriaud-Kolar, N., and Skaltsounis, A.-L. (2013) Glycogen phosphorylase inhibitors: a patent review (2008–2012). *Expert Opin. Ther. Pat.* **23,** 1017–1032
31. Vaidya, H. B., Ahmed, A. A., Goyal, R. K., and Cheema, S. K. (2013) Glycogen phosphorylase-a is a common target for anti-diabetic effect of iridoid and secoiridoid glycosides. *J. Pharm. Pharm. Sci.* **16,** 530–540
32. Agius, L. (2010) Physiological control of liver glycogen metabolism: lessons from novel glycogen phosphorylase inhibitors. *Mini Rev. Med. Chem.* **10,** 1175–1187
33. Barford, D., and Johnson, L. N. (1992) The molecular mechanism for the

tetrameric association of glycogen phosphorylase promoted by protein phosphorylation. *Protein Sci.* **1,** 472–493
34. Pfeiffer-Guglielmi, B., Fleckenstein, B., Jung, G., and Hamprecht, B. (2003) Immunocytochemical localization of glycogen phosphorylase isozymes in rat nervous tissues by using isozyme-specific antibodies. *J. Neurochem.* **85,** 73–81
35. López-Ramos, J. C., Duran, J., Gruart, A., Guinovart, J. J., and Delgado-García, J. M. (2015) Role of brain glycogen in the response to hypoxia and in susceptibility to epilepsy. *Front. Cell Neurosci.* **9,** 431
36. Duran, J., Gruart, A., García-Rocha, M., Delgado-García, J. M., and Guinovart, J. J. (2014) Glycogen accumulation underlies neurodegeneration and autophagy impairment in Lafora disease. *Hum. Mol. Genet.* **23,** 3147–3156
37. Cloix, J.-F., and Hévor, T. (2009) Epilepsy, regulation of brain energy metabolism and neurotransmission. *Curr. Med. Chem.* **16,** 841–853
38. Cloix, J.-F., and Hévor, T. (2011) Glycogen as a putative target for diagnosis and therapy in brain pathologies. *ISRN Pathol.* **2011,** 1–17
39. Xu, L., and Sun, H. (2010) Pharmacological manipulation of brain glycogenolysis as a therapeutic approach to cerebral ischemia. *Mini-Rev. Med. Chem.* **10,** 1188–1193
40. Maddaiah, V. T., and Madsen, N. B. (1966) Kinetics of purified liver phosphorylase. *J. Biol. Chem.* **241,** 3873–3881
41. Rose, R. J., Damoc, E., Denisov, E., Makarov, A., and Heck, A. J. (2012) High-sensitivity Orbitrap mass analysis of intact macromolecular assemblies. *Nat. Methods* **9,** 1084–1086
42. Kabsch, W. (2010) XDS. XDS. *Acta Crystallogr. D Biol. Crystallogr.* **66,** 125–132
43. McCoy, A. J., Grosse-Kunstleve, R. W., Adams, P. D., Winn, M. D., Storoni, L. C., and Read, R. J. (2007) Phaser crystallographic software. *J. Appl. Crystallogr.* **40,** 658–674
44. Winn, M. D., Ballard, C. C., Cowtan, K. D., Dodson, E. J., Emsley, P., Evans, P. R., Keegan, R. M., Krissinel, E. B., Leslie, A. G., McCoy, A., McNicholas, S. J., Murshudov, G. N., Pannu, N. S., Potterton, E. A., Powell, H. R., *et al.* (2011) Overview of the CCP4 suite and current developments. *Acta Crystallogr. D Biol. Crystallogr.* **67,** 235–242
45. Biasini, M., Bienert, S., Waterhouse, A., Arnold, K., Studer, G., Schmidt, T., Kiefer, F., Gallo Cassarino, T., Bertoni, M., Bordoli, L., and Schwede, T. (2014) SWISS-MODEL: modelling protein tertiary and quaternary structure using evolutionary information. *Nucleic Acids Res.* **42,** W252–W258
46. Emsley, P., Lohkamp, B., Scott, W. G., and Cowtan, K. (2010) Features and development of Coot. *Acta Crystallogr. D Biol. Crystallogr.* **66,** 486–501
47. Murshudov, G. N., Skubák, P., Lebedev, A. A., Pannu, N. S., Steiner, R. A., Nicholls, R. A., Winn, M. D., Long, F., and Vagin, A. A. (2011) REFMAC5 for the refinement of macromolecular crystal structures. *Acta Crystallogr. D Biol. Crystallogr.* **67,** 355–367
48. Pettersen, E. F., Goddard, T. D., Huang, C. C., Couch, G. S., Greenblatt, D. M., Meng, E. C., and Ferrin, T. E. (2004) UCSF Chimera: a visualization system for exploratory research and analysis. *J. Comput. Chem.* **25,** 1605–1612

Insights into Brain Glycogen Metabolism: THE STRUCTURE OF HUMAN BRAIN GLYCOGEN PHOSPHORYLASE

Cécile Mathieu, Ines Li de la Sierra-Gallay, Romain Duval, Ximing Xu, Angélique Cocaign, Thibaut Léger, Gary Woffendin, Jean-Michel Camadro, Catherine Etchebest, Ahmed Haouz, Jean-Marie Dupret and Fernando Rodrigues-Lima

J. Biol. Chem. 2016, 291:18072-18083.
doi: 10.1074/jbc.M116.738898 originally published online July 8, 2016